IOP PUBLISHING PHYSICS IN MEDICINE AND BIOLOGY

Phys. Med. Biol. **53** (2008) 6129–6141 doi:10.1088/0031-9155/53/21/016

Superparamagnetic nanoparticle-inclusion microbubbles for ultrasound contrast agents

Fang Yang[1], Ling Li[2], Yixin Li[1], Zhongping Chen[1], Junru Wu[3] and Ning Gu[1]

[1] State Key Laboratory of Bioelectronics, Jiangsu Laboratory for Biomaterials and Devices, School of Biological Science and Medical Engineering, Southeast University, Nanjing, 210096, Peoples Republic of China
[2] Ultrasound Diagnostic Department of Zhong Da hospital, Nanjing, 210096, Peoples Republic of China
[3] Physics Department, University of Vermont, Burlington, VT 05405, USA

E-mail: yangfang2080@yahoo.com.cn, nanjingliling@ sina.com, liyixin_seu@yahoo.com.cn, czp321@seu.edu.cn, jun-ru.wu@uvm.edu and guning@seu.edu.cn

Received 15 January 2008, in final form 26 August 2008
Published 14 October 2008
Online at stacks.iop.org/PMB/53/6129

Abstract

We have developed a new type of ultrasound (US) contrast agent, consisting of a gas core, a layer of superparamagnetic iron oxide Fe_3O_4 nanoparticles (SPIO) and an oil in water outermost layer. The newly developed US contrast agent microbubbles have a mean diameter of 760 nm with a polydisperity index (PI) of 0.699. Our *in vitro* and *in vivo* experiments have shown that they have the following advantages compared to gas-encapsulated microbbubbles without SPIO inclusion: (1) they provide better contrast for US images; (2) the SPIO-inclusion microbubbles generate a higher backscattering signal; the mean grey scale is 97.9, which is 38.6 higher than that of microbubbles without SPIO; and (3) since SPIO can also serve as a contrast agent of magnetic resonance images (MRI) *in vitro*, they can be potentially used as contrast agents for double-modality (MRI and US) clinical studies.

(Some figures in this article are in colour only in the electronic version)

1. Introduction

Ultrasound medical imaging is a well-established clinical diagnostic technique. However, its applications are circumscribed by its low contrast compared with other medical modalities such as MRI and x-ray (Cosgrove 2006). The contrast limitation has led to the development of ultrasound contrast agents (UCAs). These contrast agents are usually gas-filled bubbles of micron size; they offer high acoustic impedance mismatch with tissues in ultrasound imaging (Margaret *et al* 2006); the gas, usually encapsulated by a shell, can be air, nitrogen,

perfluorocarbon, sulfur hexafluoride and other inert gas or gas mixture (Schutt *et al* 2003). Several cardiac and vascular UCAs are now commercially available; for example, they are Optison® (GE Healthcare, Princeton, NJ, USA), Definity® (Lantheus Medical Imaging, N. Billerica, MA) and Levovist® (Schering AG, Berlin, Germany). Among them, Optison® has been approved by the Food & Drug Administration (FDA) for the clinical applications in the USA; it contains micron-size denatured albumin microspheres filled with octafluoropropane. Ultrasound imaging assisted by UCAs, which can be easily injected intravenously during clinical applications, has the following attractive features: (1) it is a relatively noninvasive, low-risk and real-time imaging technique (Correas *et al* 2001, Pisani *et al* 2006) and (2) UCAs such as Optison® can be persistent in the blood stream after the injection for enough time for imaging because the core gas (octafluoropropane) has low solubility and diffusivity in blood (Wheatleya *et al* 2006).

The interaction of ultrasound with microbubbles has been studied extensively in order to understand the mechanism of contrast enhancement, improve contrast agent detection and guide the development of more new effective contrast agents. Generally speaking, the UCAs should be of micron or submicron size and highly echogenic. The submicron size distribution can provide applications in targeting molecular imaging experiments. UCAs whose diameters were less than 900 nm were used to bind to the target (Hughes and Marsh 2005, Kheirolomoom *et al* 2007, Oeffinger *et al* 2004). Small-diameter bubbles can have a prolonged lifetime in circulation, and they can increase numbers passing through tumour vasculature to achieve satisfactory tumour-targeting imaging (Bloch *et al* 2004, Liu *et al* 2006). Nowadays, several new types of UCAs have been suggested including liquid-filled microemulsions and nanoemulsions, liposomes and some nanoparticles with acoustic impedance mismatched from soft tissue (Alexander 2005). Nanoparticles used as UCAs have drawn a large degree of interest as targeted imaging and therapeutic agents because of their unique small sizes and high tissue extravasation rates. Liu *et al* (2006) investigated the feasibility of using silica nanosphere solid nanoparticles as UCAs for ultrasonic imaging. In an animal experiments, originally designed for MRI applications, Nolte *et al* (2005) demonstrated that they were able to detect superparamagnetic iron oxide Fe_3O_4 (SPIO) nanoparticles ultrasonically, which had been pre-injected in the brain tumour of a monkey as MRI contrast agents, using a high frequency intra-operative ultrasound transducer. They further confirmed the diagnosis of the tumour ultrasonically by MRI. Oh *et al* (2006) in a similar animal experiment also found that the backscattering ultrasound signal increased with increasing SPIO doses. Other submicron solid nanoparticles that were evaluated both *in vitro* (tissue phantom) and *in vivo* (mice) include silica and polystyrene nanoparticles (Norton and Vo-Dinh 2007, Anton *et al* 2002). All the above-mentioned studies illustrate that the use of solid nanoparticles can enhance the contrast for ultrasound B-mode images.

The objectives of this study were twofold. First, we developed multiple emulsion-stabilized microbubbles of submicron sizes with inclusions of SPIO. Secondly, since it was reported that SPIO can also serve as a contrast agent for MRI *in vitro*, we wanted to verify whether our multiple emulsion-stabilized microbubbles with inclusions of SPIO could be potentially used as contrast agents for double-modality (MRI and US) clinical studies.

The structure of the microbubbles that were developed can be briefly described as follows: the core gas of the first emulsion microbubble was N_2, encapsulated by a shell of poly-d,l-lactide (PLA) of good biocompability and biodegradability (Pisani *et al* 2006). SPIO nanoparticles were added during the formation of the first bubble emulsion. The second shell was poly(vinyl alcohol), PVA, a synthetic polymer with good biocompatibility properties (Cavalieri *et al* 2005, 2006, Paradossi *et al* 2002, Rota *et al* 2006, Diaz-Castanon 2008).Our SPIO-inclusion microbubbles used in *in vitro* (phantom) and *in vivo* (animal) experiments showed that they

enhanced the image contrast for US imaging and potentially could be used to increase the contrast of MRI as well.

2. Materials and methods

2.1. Materials

Poly(d,l-lactide) (7000 MW), PLA, was purchased from Shandong Key Laboratory of Medical Polymer Materials. Poly(vinyl alcohol), PVA, 88 mol% hydrolyzed with a MW of 25 000 was from Alfa Aesar®. Superparamagnetic iron oxide Fe_3O_4 nanoparticles with a mean diameter of 10 nm were from Jiangsu Laboratory for Biomaterials and Devices as a gift. Span 80 (sorbitan monostearate), Tween 80 (polyoxyethylene sorbitan monooleate), N_2 and other chemicals were reagent grade. Water was purified using a Milli-Q system from Millipore (Millipore, France) to purity grade (18 MΩ cm).

2.2. Preparation of Fe_3O_4/PLA/ N_2 microbubbles

An organic solution (10.00 ml) was prepared containing PLA (0.50 g) and hydrophobic SPIO nanoparticles (0.05 g) in methylene chloride at 25 °C. To first generate SPIO-inclusion bubble emulsion, 1.00 mL Milli-Q water and 0.50 ml Tween 80 were added to the organic solution and continuously sonicated at 100 W with a probe while constantly purging using a steady (4 ml min^{-1}) stream of N_2 gas for 5 min. The bubble emulsion was brown and visibly homogeneous. The dissociated Fe_3O_4 nanoparticles were separated from the first emulsion bubble solution under an external optimal magnetic field.

The first bubble emulsion was then poured into a 1% PVA (w/v) solution and mixed mechanically for 2 h to form stable multiple emulsion bubbles. After reaction, the final emulsion became milk-white.

2.3. Separation of multiple emulsion microbubbles from larger bubbles

The multiple emulsion bubble solution was transferred to a custom-made centrifuge tube. Suspended bubbles were centrifuged for 5 min at 500 rpm. In most cases, the solution was separated into two distinct layers: the upper layer containing mostly large bubbles and the lower layer containing nanometre bubbles in the solution. The lower layer of the solution was collected for size and acoustic analysis, and the top layer was discarded. If no distinct layer was observed, 5.0 ml (consistent with layered samples) was collected from the bottom of the centrifuge tube. The collected agent was stored at 4 °C in tightly capped vials sealed with paraffin films. Before the sample was used, it was diluted 1:1 in sterile saline. Figure 1 is the schematic diagram of a multiple emulsion microbubble.

2.4. Characterization

The mean diameter size of the bubbles was analysed using the N4 PLUS submicron particle size analyser (Beckman Coulter, USA). The measure angle was 90.0°. The particle size distribution was determined by using PCS control software which was a part of built-in software of the particle size analyser. Milli-Q pure water was used as the blank solution, and the sample was added until an appropriate concentration was indicated. Each sample was tested in triplicate.

Samples in solution were placed between glass slides and observed with an Axioskop 40 microscope equipped with a Coolsnap MP3.3 camera (Carl Zeiss, Germany). Because the

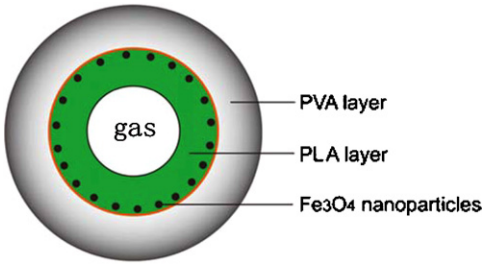

Figure 1. The schematic diagram of the PVA/Fe_3O_4/PLA multiple emulsion microbubbles.

typical sample particle size was of the order of 800 nm, an oil immersion lens was used for viewing.

In order to verify whether or not the superparamagnetic Fe_3O_4 nanoparticles were encapsulated into the microbubbles, their morphology and structure were determined by transmission electron microscopy (TEM). It was found that most nanoparticles were present between the two shells of the microbubbles, and the results have been reported elsewhere (Yang *et al* 2008).

The magnetization properties at room temperature (20 °C) of the SPIO-inclusion microbubbles was further studied by using a 7407 vibrating sample magnetometer (VSM) (Lake Shore Cryotronics, Inc., OH, USA). The samples included the SPIO-inclusion microbubbles and the microbubbles without SPIO inclusions. All the tested samples were dried at 80 °C prior to analysis. Due to the extremely low magnetic moments of the samples, the correct hysteresis loops were obtained after subtracting the offset background signals using the procedure suggested by the manufacturer's instruction manual. Saturation magnetization, coercive force and remnant magnetization were obtained from the hysteresis loops. Specifically, the saturation magnetization (Ms) and remnant magnetization (Mr) were obtained by extrapolation of the hysteresis loops to the infinite field of the experimental data obtained in the high field range where the magnetization varies linearly with the inverse of the applied field. Each sample was measured in triplicate.

2.5. In vitro acoustic imaging test

In vitro ultrasound imaging analysis (Kinoshita and Hynynen 2007) was performed by using a home-made stimulated setup. Figure 2 shows a schematic diagram of the experimental setup. The setup consisted of a water reservoir with a spherical sample pool, a peristaltic pump with a flow speed of 10 μl s^{-1} and a microbubble sample injector. The dimension of spherical sample pool was 1 cm in central diameter and was positioned in the middle of the water reservoir filled with de-gassed and de-ionized water, vertically relative to the ultrasound transducer. First, the de-gassed and de-ionized water was cycled by the peristaltic pump through the whole system to simulate the *in vivo* dynamic blood flow process. When the transducer was inserted in the water reservoir to detect, the sample of microbubbles was injected by the injector simulating the process of *in vivo* perfusion. Three samples, including de-gassed water, microbubbles without SPIO-inclusion and SPIO-inclusion microbubbles, were imaged using the ultrasonic imaging system of the GE LOGIQ9 scanner (GE Medical Systems, USA) with a 3.5 MHz ultrasound transducer used as a transmitter as well as a receiver. All images were acquired with the same instrument parameters (mechanical index (MI) = 0.1; gain = 10 dB).

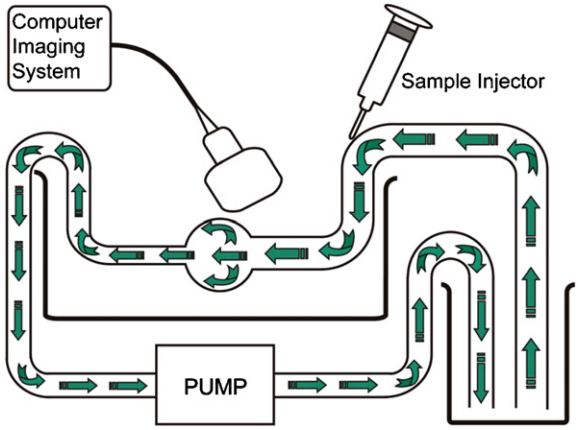

Figure 2. The schematic diagram of the experimental setup *in vitro*.

2.6. In vivo experiments

All *in vivo* studies were performed according to a protocol approved by the Internal Review Board and by the animal care committee of the Southeast University. Twelve New Zealand white rabbits (of either sex), within the weight range of 3.0–5.0 kg, were used. They were selected and randomized into three groups (four rabbits every group). One group was injected with SPIO-inclusion bubbles. Another group was injected with the bubbles without SPIO inclusions. The third control animal group was used to rule out the possibility of enhancement caused by the sterile saline. Sterile saline (5 ml) was injected into the catheterized ear vein of the four rabbits that did not have any microbubbles injections. In a parallel imaging experiment, the samples with the SPIO-inclusion bubbles, and the bubbles without SPIO should have the same concentration and the same size distribution. The rabbits were anaesthetized by intramuscular injections of urethane (30 mg kg^{-1}) using an 18-gauge needle, which maintained the anaesthetic effect. At the same time, the rabbits were placed in dorsal recumbency on a heated imaging table (37 °C). Following anaesthesia, the ventral chest area was shaved and depilated to minimize the entrapment of air bubbles on the skin during ultrasound scanning. Heart rate and body temperature were monitored using electrocardiograph (ECG) leads attached to the four limbs and a rectal probe, respectively. The contrast agents were suspended in the sterile saline in a 1:1 ratio and were injected intravenously during an ultrasonic examination. The agents had a final concentration of 2.7×10^8 microbubbles ml^{-1}. For each single injection, a syringe with a 18-gauge needle was used to draw the bubbles solution according to each rabbit body weight. The dose was of 1 ml microbubbles/kg body weight. The suspension was then diluted to the fixed 5 ml volume for each single injection through a catheterized ear vein of rabbit within 1 min. Immediately after administration the injection port was flushed with 1 ml of saline. Ultrasound contrast imaging of the liver was then performed using a GE LOGIQ9 scanner. A high bandwidth (5–12 MHz) linear array transducer (M12L, 10 MHz) was used to scan the liver and the images were recorded as digital files. The *in vivo* effects of the microbubbles were studied by monitoring the image change in the rabbit's liver after intravenous administration. To optimize the chance of acquiring identical imaging during the entire experiment, the transducer was fixed and the rabbits were kept under continuous anaesthesia. Frame images were acquired from 0 to 15 min and at every 1 min interval after injection. All imaging parameters were kept unchanged

during the entire imaging experiment (MI: 0.1; gain = 4 dB) at the same anatomic site when the livers were momentarily stationary (Quaia *et al* 2006). The same longitudinal scan plane through the liver was used in all cases.

2.7. Mean grey scale analysis

To quantitatively measure image brightness, a mean grey scale was calculated as the average of the grey scale levels of all pixels within a region of interest (ROI). The images were digitized at an 8-bit resolution; thus, the range of pixel grey scale levels was 0–255. The manual definition of ROI was allowed. The calculations of mean grey scale within defined ROIs were done. To reduce potential bias in performing ROI selection, a MatLab computer program was developed to automatically define the ROIs at fixed positions for all frame images, and the mean grey scale for each ROI was calculated accordingly. In *in vitro* experiments, the same oval ROIs within the focal zones were defined on the images. The ROIs for all animal liver images were rectangular with 3.97 mm in width and 2.54 mm in height. The mean grey scales within the ROIs were calculated for comparison.

2.8. In vitro magnetic resonance imaging (MRI)

De-gassed and de-ionized Millipore water, SPIO-inclusion bubbles, bubbles without SPIO inclusions and bubbles with the same concentration of SPIO outside the bubbles were placed in four eppendorf tubes of 1 cm in diameter. MRI of these tubes was performed with a clinical 1.5 T MR imager (Eclipse, Philips Medical Systems, The Netherlands) by using a 12.7 cm long receive-only surface coil. The MRI sequences were a T1 (spin–lattice interaction time constant)-weighted spin-echo (repetition time (ms)/echo time (ms), 500/17.9), a T2 (spin–spin interaction time constant)-weighted fast spin-echo (4000/108; echo train length, 16) and a T2*-weighted (T2*WI) gradient-echo (620/15.7; flip angle, 35°) sequence. Images were obtained with a matrix size of 256 × 256, section thickness of 2 mm and field of view of 10 × 10 cm^2. Three separate measurements were acquired of each sample for the three different pulse sequences. The area of the ROI for signal intensity (SI) measurement was 20 mm^2. The percentage change of SI was calculated using the following equation:

$$\delta(\mathrm{SI}) = (\mathrm{SI}_{\mathrm{sample}} - \mathrm{SI}_{\mathrm{blank}})/\mathrm{SI}_{\mathrm{blank}} \times 100\% \quad (1)$$

where $\mathrm{SI}_{\mathrm{sample}}$ and $\mathrm{SI}_{\mathrm{blank}}$ were the SIs of the microbubbles and de-gassed and de-ionized Millipore water, respectively.

3. Results and discussion

3.1. Characterization of Fe_3O_4/PLA/ N_2 multiple emulsion stable microbubbles

The mean diameter size (each sample for triplicate) was found to be about 700–800 nm and the size distribution was slightly asymmetric, as shown in figure 3. The mean diameter of all microbubble samples was calculated to be 760 nm with a polydisperity index (PI) of 0.699, very much the same as that of the size distribution of microbubbles without SPIO. This result suggests that the addition of SPIO in the polymer spheres did not significantly affect microbubble size distribution.

The size distribution was also estimated under light microscopic observation using an oil-coupled 100× objective lens (figure 4). They ranged from 500 to 1000 nm in the suspension solution; bubbles smaller than 500 nm could not be resolved by this type of technique. The microscopic images indicate the regular spherical morphology.

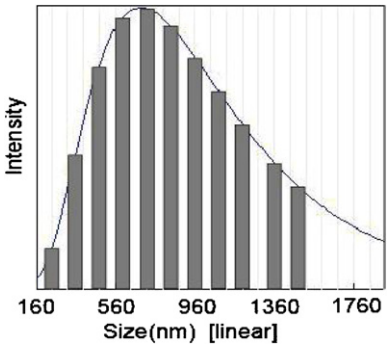

Figure 3. The relative size distribution of the microbubble was measured by the N4 PLUS submicron particle size analyser. The mean diameter of the microbubble was 760 nm with the size distribution of polydisperity index (PI) of 0.699. The intensity scale on the *y*-axis represented the volume fractions of each size.

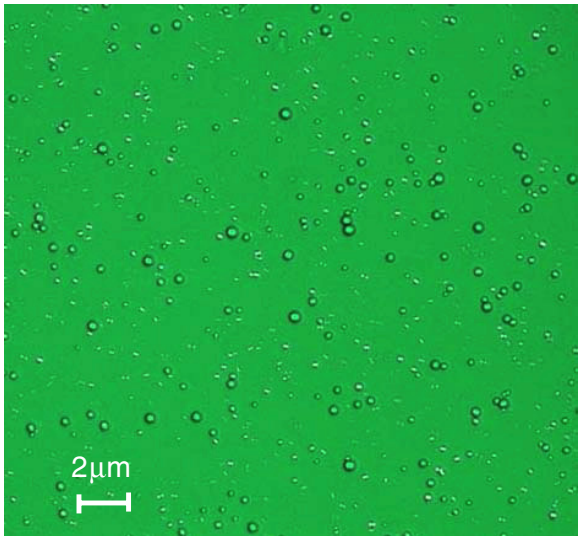

Figure 4. Microscopy image of SPIO microbubbles in bright fields under the oil immersion lens.

Figure 5 shows the magnetization properties of the SPIO-inclusion microbubbles. Their magnetization VSM curve looks the same as that of magnetic nanoparticles of 10 nm size in the hydrophobic magnetite gel measured by Liu *et al* (2007). There is no remnant magnetization observed in the VSM curve (figure 5), indicating that the inclusion material preserved superparamagnetic characteristics at room temperature. As a control, we demonstrated (not shown here) that the VSM curve was not obtained in the microbubbles without SPIO inclusion.

3.2. In vitro acoustic testing

The ultrasound images of the de-gassed and de-ionized water, the multiple emulsion microbubbles without SPIO and the multiple emulsion microbubbles with SPIO were captured;

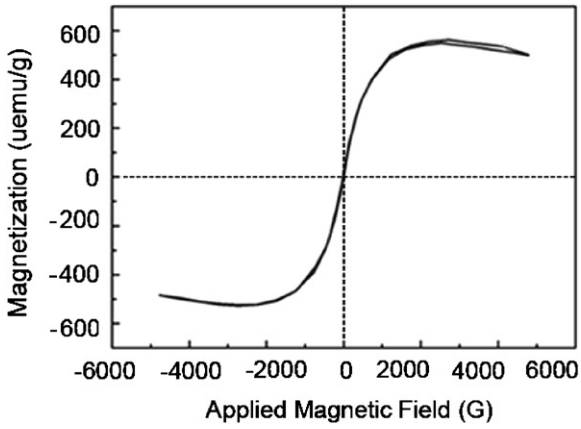

Figure 5. VSM curve of synthesized PVA/Fe_3O_4/PLA/N_2 multiple emulsion micobubbles.

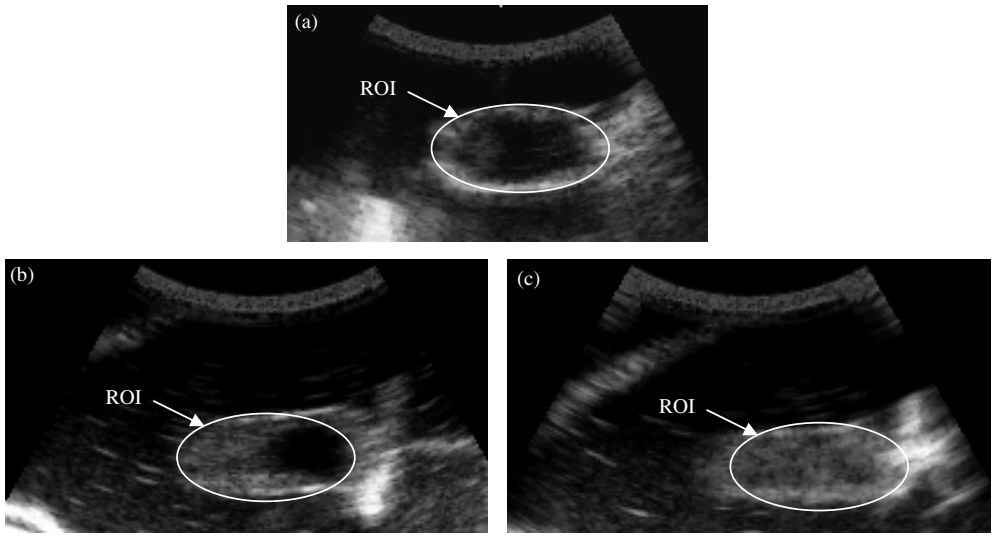

Figure 6. The *in vitro* ultrasound imaging in the different phantom samples: (a) de-gassed and de-ionized water; (b) the multiple emulsion microbubbles without Fe_3O_4 nanoparticles; (c) the multiple emulsion microbubbles with Fe_3O_4 nanoparticles.

they are shown in figures 6(a)–(c), respectively. Compared with figure 6(a) of the de-gassed and de-ionized water, the brighter area can be seen distinctly in the multiple emulsion microbubbles without SPIO and the multiple emulsion microbubbles with SPIO. The results also show that the image of the multiple emulsion microbubbles with SPIO (figure 6(c)) is brighter than that of the multiple emulsion microbubbles without SPIO (figure 6(b)). It suggests that the inclusion SPIOs also contributed to ultrasound backscattering echo intensity. The mean grey scales within the ROIs of the de-gassed and de-ionized water images, the multiple emulsion microbubbles without SPIO and the multiple emulsion microbubbles with SPIO are 25.4, 59.3 and 97.9, respectively. (The results are shown in table 1.) This result indicates that at the same concentration, SPIO-inclusion microbubbles had 38.6 greater mean grey scale

Table 1. The mean grey scale within ROI measured by using an ultrasound imaging system. Three replicates were measured for each sample. The data are presented as mean ± standard deviation.

Samples	De-gassed and de-ionized water	Microbubbles without SPIO	Microbubbles with SPIO
Mean grey scale	25.4 ± 1.8	59.3 ± 2.9	97.9 ± 2.1

enhancement than microbubbles without SPIO; the Fe_3O_4 nanoparticles also had contributions to the ultrasound imaging enhancement.

3.3. SPIO-inclusion microbubbles ultrasound imaging enhancement

The *in vitro* experiment showed that for the same concentration and size distribution, SPIO-inclusion microbubbles had greater mean grey scale reading than microbubbles without SPIO. Raisinghani and Stride (Raisinghani and DeMaria 2002, Stride 2008) contributed the enhancement to the multiple shell or other substance existing in the shell which altered the surface tension of a microbubble; the enhancement is particularly useful for lengthening imaging duration and improvement of imaging quality. In order to understand the different efficacy of SPIO-inclusion microbubbles and microbubbles without SPIO inclusion, the backscattered signal intensity *in vitro* over a wide range of concentrations was measured according to the comparison experiments (Bouakaz *et al* 1998). It was observed that microbubbles with SPIO inclusion could give higher signal intensity than microbubbles without SPIO inclusion. This result indicates that the SPIO inclusion in the shell may substantially modify the amplitude of microbubbles volumetric oscillation, resonance characteristics and relative amplitude in tension and compression under the same ultrasound imaging conditions. We think both the polymer shell and the SPIO nanoparticles in the shell may attribute to boost the acoustic impedance resulting in stronger scattering signals; i.e. the SPIO-inclusion microbubbles may cause stronger backscatter signals during imaging.

3.4. Animal liver ultrasound imaging results

In *in vivo* animal studies, ultrasound phase inversion contrast mode imaging of a rabbit's liver was acquired as shown in figure 7. The substantial contrast enhancement was observed with the injected contrast agent (microbubbles with SPIO) compared to the image of the control case obtained pre-injection of the contrast agent. After intravenous injection of the multiple emulsion microbubbles in the rabbit, the brightness in the liver increased over the time. Figure 7 shows an example of the reflectivity enhancement by comparing two images: one was acquired at the beginning of the injection and the other was acquired at 5 min after injection. Control rabbits injected with saline did not show any change in the mean grey scale within the liver ROI over the duration of the imaging period. The control rabbits injected with bubbles without SPIO had a different change from those with SPIO-inclusion bubbles. The comparison of the mean grey scale between the SPIO-inclusion bubbles and the bubbles without SPIO under the same conditions is shown in figure 8.

Each time point of each curve in figure 8 was the mean data from one experimental animal group images (four rabbits). Figure 8(a) is the mean grey scale change plot of SPIO-inclusion bubbles over time (0 to 15 min, every 1 min increment). It was found that within the first 1 min after injection, the grey scale increased rapidly. Then the brightness of images increased gradually until 11 min. Between 11 min and 15 min, the mean grey scale began to gradually

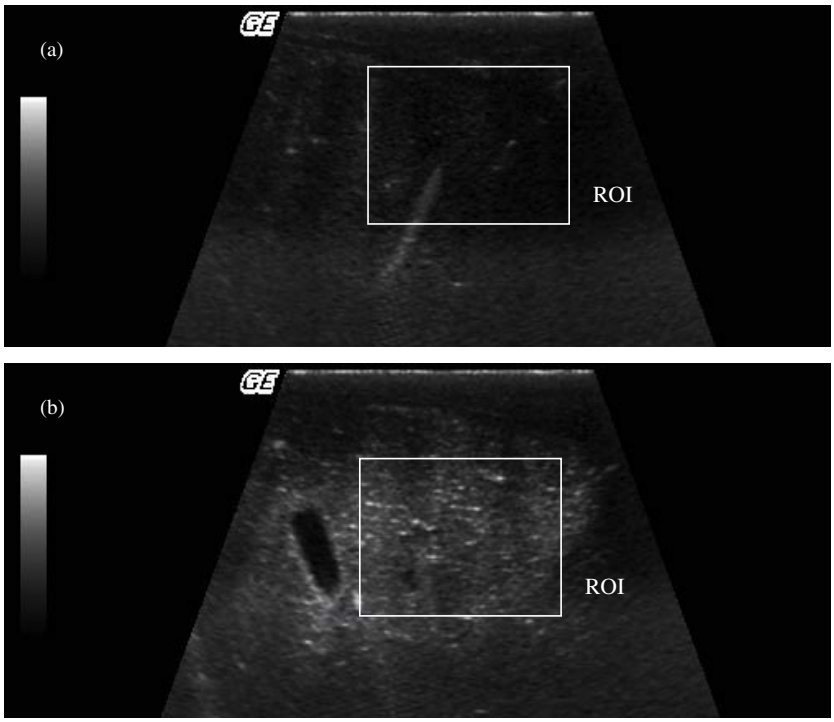

Figure 7. Ultrasound image of a rabbit's liver showing the enhanced contrast by using SPIO microbubbles. (a) Conventional ultrasound image pre-injection of the microbubble contrast agent and (b) post-injection (after 5 min) of the microbubble contrast agent (5 ml, 2.7 × 10^8 bubbles ml^{-1}).

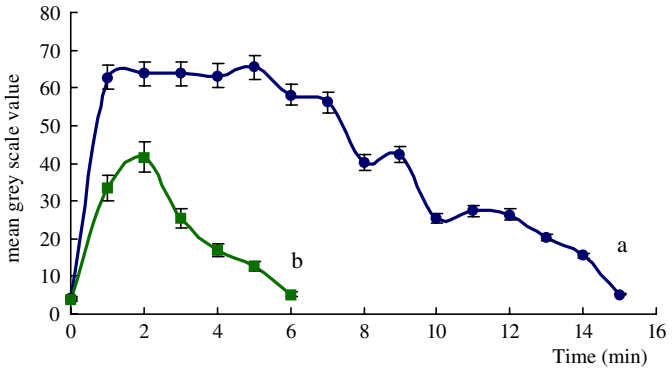

Figure 8. (a) The mean grey scale in a rabbit's liver versus time after SPIO-inclusion bubbles were injected. (b) The mean grey scale in a rabbit's liver versus time after bubbles without SPIO were injected. The enhancement of the ultrasound imaging was changed over the time. The data of the curve were obtained by statistical analysis from the four rabbits of each group.

decrease. The plateau in figure 8, curve (a), may result from the retention of submicron size bubbles and the aggregation of SPIO nanoparticles releasing from some microbubbles. The

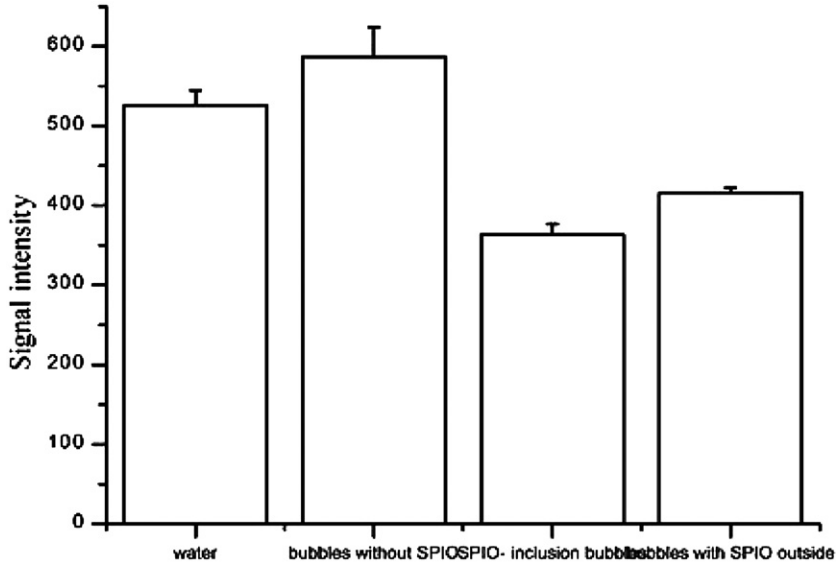

Figure 9. Bar graph showed the mean signal intensity of T2*WI. There was a significant signal intensity decrease of the SPIO-inclusion microbubbles sample *in vitro* which is the basis of the contrast enhancement of MRI applications.

delayed and persistent enhancement of normal liver parenchyma appeared to be caused by the phagocytosis of intact submicron-size bubbles and the released SPIO nanoparticles by Kupffer cells. Thus, the deposition of some bubbles and SPIO nanoparticles may have great advantages for the longer imaging persistence and following MRI applications. Figure 8(b) is the mean grey scale change plot of bubbles without SPIO over time (0 to 6 min). Those bubbles without SPIO had shorter image enhancement duration time than the SPIO-inclusion bubbles. *In vivo* experiments have also shown that the SPIO-inclusion bubbles have better image enhancement. Therefore, the SPIO indeed had the contributions to the ultrasound imaging enhancement. After the bubbles were destroyed at MI $\geqslant 0.8$ using pulse inversion imaging, the SPIO was released from the bubbles and aggregated in the tissue, which resulted in the long-lasting brightness of the ultrasound imaging.

3.5. In vitro MRI results

The MRI pulse sequences of T1-, T2- and T2*-weighted (T2*WI) were all performed. The data showed that there was almost no change in the T1 signal. The T2 and T2*WI signals were changed; especially the T2*WI signal intensity was reduced significantly. Therefore, the T2*-weighted (T2*WI) gradient-echo MR bar chart of the samples is shown in figure 9. The vertical axis represents a relative reading of T2*WI which demonstrates a significant decrease of SI for SPIO-inclusion microbubbles compared with the microbubble solution without SPIO. According to equation (1), the mean δ (SI) value of SPIO-inclusion microbubbles was calculated to be $31.0 \pm 5.8\%$ ($n = 3$) reduction (=(362.95–526.03)/526.03)). The mean δ (SI) value of bubbles with the same concentration of SPIO outside of the bubbles was calculated to be $20.9 \pm 4.7\%$ ($n = 3$) reduction (=(416.16–526.03)/526.03)). The result indicated that there were different influences affecting relaxivity between bubbles with the same concentration of SPIO outside of the bubbles and the SPIO-inclusion microbubbles. It seems that increasing the

magnetic susceptibility of the shell by embedding magnetically active particles, such as SPIO nanoparticles, is equivalent to increasing the susceptibility difference between the bubble and its environment. The *in vitro* MRI experiment demonstrates that the SPIO-inclusion microbubbles also play a role as contrast agents for MRI.

4. Summary

In this study, we synthesized multilayer emulsion microbubbles of mean diameter 760 nm containing SPIO in the oil layer and a core filled with N_2 gas. The *in vitro* and *in vivo* experiments show that inclusion of SPIO enhanced the contrast of US images compared to that of the gas-encapsulated microbubbles without SPIO. This effect may be due to the fact that the aggregates of SPIO in microbubbles provided additional acoustic impedance mismatch with soft tissue compared to microbubbles without SPIO during the ultrasound imaging.

The *in vitro* MRI experiment shows that microbubbles with SPIO also enhanced the contrast of MRI. Thus, the accumulation of the Fe_3O_4 in the tissues could also be used in MRI as well as US imaging. Therefore, SPIO-inclusion microbubbles can potentially be used as contrast agents for double-modality (MRI and US) clinical studies. Our work is preliminary although encouraging; further *in vitro* and *in vivo* studies will be necessary before they can be used as new UCAs clinically.

Acknowledgments

This investigation was supported in part by the National Important Science Research Program of China (no 2006CB933206) and National Natural Science Foundation of China (nos 60371027, 60171005 and 90406023). The study was also obtained the partial financial aid from the Scientific Research Foundation of Graduate School of Southeast University.

References

Alexander L Klibanov 2005 Ligand-carrying gas-filled microbubbles: ultrasound contrast agents for targeted molecular imaging *Bioconjug. Chem.* **16** 9–17

Anton M, Schillinger U, Henke J and Bergermann C 2002 Magnetofection: enhancing and targeting gene delivery by magnetic force *in vitro* and *in vivo Gene Ther.* **9** 102–9

Bloch S H, Dayton P A and Ferrara K 2004 Targeted imaging using ultrasound contrast agents *IEEE Eng. Med. Biol. Mag.* **23** 18–29

Bouakaz A, De Jong N and Cachard C 1998 Standard properties of ultrasound contrast agents *Ultrasound Med. Biol.* **24** 469–72

Cavalieri F, Hamassi A E, Chiessi E and Paradossi G 2005 Stable polymeric microballoons as multifunctional device for biomedical uses: synthesis and characterization *Langmuir* **1** 8758–64

Cavalieri F, Hamassi A E, Chiessi E and Paradossi G 2006 Tethering functional ligands onto shell of ultrasound active polymeric microbubbles *Biomacromolecules* **7** 604–11

Correas J-M, Bridal L, Lesavre A, Mejean A, Claudon M and Helenon O 2001 Ultrasound contrast agents: properties, principles of action, tolerance, and artifacts *Eur. Radiol.* **11** 1316–28

Cosgrove D 2006 Ultrasound contrast agents: an overview *Eur. J. Radiol.* **60** 324–30

Diaz-Castanon S, Faloh-Gandarilla J C, Munoz-Sandoval E and Terrones M 2008 Vibration sample magnetometry, a good tool for the study of nanomagnetic inclusions *Superlattices Microstruct.* **43** 482–6

Hughes M S and Marsh J N 2005 Acoustic characterization in whole blood and plasma of site-targeted nanoparticle ultrasound contrast agent for molecular imaging *J. Acoust. Soc. Am.* **117** 964–72

Kheirolomoom A, Dayton P A, Aaron F, Lum H, Little E, Paoli E E, Zheng H and Ferrara K W 2007 Acoustically-active microbubbles conjugated to liposomes: characterization of a proposed drug delivery vehicle *J. Control. Release* **118** 275–84

Kinoshita M and Hynynen K 2007 Key factors that affect sonoporation efficiency in *in vitro* settings: the importance of standing wave in sonoporation *Biochem. Biophys. Res. Commun.* **359** 860–5

Liu J, Levine A L, Mattoon J S, Yamaguchi M, Lee R J, Pan X and Rosol T J 2006 Nanoparticles as imaging enhancing agents for ultrasonography *Phys. Med. Biol.* **51** 2179–89

Liu X, Kaminski M D, Chen H, Torno M, Taylor L A and Rosengart J 2007 Synthesis and characterization of highly-magnetic biodegradable poly(D,l-lactide-co-glycolide) nanospheres *J. Control. Release* **119** 52–8

Margaret A Wheatley, Flemming Forsberg, Kelleny Oum, Raymond Ro and Dalia El- Sherif 2006 Comparison of *in vitro* and *in vivo* acoustic response of a novel 50:50 PLGA contrast agent *Ultrasonics* **44** 360–367

Nolte I, Vince G H, Maurer M, Herbold C, Goldbrunner R, Solymosi L, Stoll G and Bendszus M 2005 Iron particles enhance visualization of experimental gliomas with high-resolution sonography *Am. J. Neuroradiol.* **26** 1469–74

Norton S J and Vo-Dinh T 2007 Imaging the distribution of magnetic nanoparticles with ultrasound *IEEE Trans. Med. Imaging* **26** 660–5

Oeffinger B E, Margaret A and Wheatley A 2004 Development and characterization of a nano-scale contrast agent *Ultrasonics* **42** 343–7

Oh J, Feldman M D, Kim J, Condit C, Emelianov S and Milner T E 2006 Detection of magnetic nanoparticles in tissue using magneto-motive ultrasound *Nanotechnology* **17** 4183–90

Paradossi G, Cavalieri F, Chiessi E, Ponassi V and Martorana V 2002 Tailoring of physical and chemical properties of macro- and microhydrogels based on telechelic PVA *Biomacromolecules* **3** 1255–62

Pisani E, Tsapis N, Paris J, Nicolas V, Cattel and Fattal E 2006 Polymeric nano/microcapsules of liquid perfluorocarbons for ultrasonic imaging: physical characterization *Langmuir* **22** 4397–402

Quaia E, Bartolotta T V, Midiri V M, Cernic S, Belgrano M and Cova M 2006 Analysis of different contrast enhancement patterns after microbubble-based contrast agent injection in liver hemangiomas with atypical appearance on baseline scan *Abdom. Imaging* **31** 59–64

Raisinghani A and DeMaria A D 2002 Physical principle of microbubble ultrasound contrast agents *Am. J. Cardiol.* **90** (suppl) 3J–7J

Rota C, Raeman C H, Child S Z and Dalecki D 2006 Detection of acoustic cavitation in the heart with microbubble contrast agents *in vivo*: a mechanism for ultrasound induced arrhythmias *J. Acoust. Soc. Am.* **120** 2958–64

Schutt E G, Klein D H, Mattrey R M and Riess J G 2003 Injectable microbubbles as contrast agents for diagnostic ultrasound imaging: the key role of perfluorochemicals *Angew. Chem. Int. Ed.* **42** 3218–35

Stride E 2008 The influence of surface adsorption on microbubble dynamics *Phil. Trans. R. Soc.* **366** 2103–15

Wheatleya M A, Forsberg F, Oum K, Ro R and El-Sherif D 2006 Comparison of *in vitro* and *in vivo* acoustic response of a novel 50:50 PLGA contrast agent *Ultrasonics* **44** 60–367

Yang F, Gu A, Chen Z, Gu N and Ji M 2008 Multiple emulsion microbubbles for ultrasound imaging *Mater. Lett.* **62** 121–4